doi:10.26443/seismica.v4i2.1682

Spatially heterogenous Holocene slip rates drive seismic sequence variability on a normal fault

Constanza Rodriguez Piceda [*1], **Zoë K. Mildon** [1], **Billy J. Andrews** [1], **Francesco Visini** [2], **Jean-Paul Ampuero** [3], **Martijn van den Ende** [3]

[1]University of Plymouth, School of Geography, Earth and Environmental Sciences, Plymouth, United Kingdom, [2]National Institute of Geophysics and Volcanology (INGV), Italy, [3]Université Côte d'Azur, Observatoire de la Côte d'Azur, IRD, CNRS, Géoazur, Nice, France

Author contributions: *Conceptualization*: C. Rodriguez Piceda, Z. Mildon, B. Andrews. *Methodology*: C. Rodriguez Piceda, Z. Mildon, B. Andrews, F. Visini. *Software*: C. Rodriguez Piceda, J. P. Ampuero, M. van den Ende. *Validation*: C. Rodriguez Piceda, Z. Mildon, B. Andrews, F. Visini, J. P. Ampuero, M. van den Ende. *Formal Analysis*: C. Rodriguez Piceda, Z. Mildon, B. Andrews. *Investigation*: C. Rodriguez Piceda, Z. Mildon, B. Andrews. *Resources*: Z. Mildon. *Writing - Original Draft*: C. Rodriguez Piceda. *Writing - Review & Editing*: C. Rodriguez Piceda, Z. Mildon, B. Andrews, F. Visini, J. P. Ampuero, M. van den Ende. *Visualization*: C. Rodriguez Piceda. *Project Administration*: Z. Mildon. *Funding Acquisition*: Z. Mildon.

Abstract Spatial variations in long-term (e.g. Holocene) slip rates along faults are a source of uncertainty in fault-based seismic hazard assessment (SHA), but their effect on seismicity rates and magnitude-frequency distributions remains underexplored. We conduct numerical simulations of earthquake cycles on the Parasano-Pescina normal fault in Central Italy, using multiple along-strike slip rate measurements, to investigate how spatial variations in slip rate influence slip modes, rupture extent, seismicity rates and magnitudes. We compared synthetic catalogs generated using different profiles with variable slip rates with those based on a single measurement and estimated associated ground-shaking intensities. Profiles with variable slip rate affect earthquake magnitude and recurrence by modulating stress accumulation. Highly variable slip rate profiles lead to more complex rupture patterns, including partial ruptures and slow slip events, contributing to variability in stress distribution in earthquake recurrence, magnitude-frequency distributions and ground-shaking intensities. Simplified slip rate profiles based on a single measurement produce less realistic seismic catalogues with earthquakes of characteristic magnitude and regular recurrence. This highlights the need for detailed profiles to improve SHA, particularly for faults with relatively limited rate-and-state weakening behavior and sharp along-strike gradients in long-term slip rate.

Production Editor:
Andrea Llenos
Handling Editor:
Alexandra Hatem
Copy & Layout Editor:
Anna Ledeczi

Signed reviewer(s):
Octavi Gómez Novell

Received:
3 April 2025
Accepted:
25 September 2025
Published:
10 October 2025

Non-technical summary In assessing earthquake hazard, one major uncertainty is how tectonic slip rates vary along faults and how this influences the earthquake timing and size. We developed computer-based simulations of earthquakes on a fault in Italy to investigate how the spatial variations in slip rate affect earthquake behaviour and ground shaking. Models based on a single slip rate measurements produced overly simple earthquake patterns with regular timing and similar magnitudes. In contrast, models using spatially variable slip rates generates more realistic patterns, with earthquakes of different sizes and irregular recurrence. Our results show that detailed slip rate information is needed for improving seismic hazard assessments.

1 Introduction

The use of geological fault data to define seismogenic sources, including fault geometry and geologic slip rate, is a common practice in probabilistic seismic hazard assessment (Chartier et al., 2017; Field et al., 2014; Valentini et al., 2017; Williams et al., 2023; Gómez-Novell et al., 2020). One key input used in fault based SHA is the long-term (>1e3 yr) slip rate (V_g) which generally reflects the cumulative strain released by the fault across multiple seismic cycles (Cowie et al., 2012). Long-term slip rate is related to the earthquake potential of a fault by calculating the geological moment accumulation rate ($\dot{M}_g$) (Brune, 1968).

$$\dot{M}_g = GAV_g \quad (1)$$

where G is the shear modulus and A the fault seismogenic area. This method assumes that all accumulated geologic moment is released entirely by earthquakes, and that the hazard posed by the fault is represented by a single value of long-term slip rate. These assumptions enable the calculation of earthquake rates for a seismic catalog of a given moment magnitude (M_w) range and fault area from long-term slip rates (Field et al., 1999).

Geological observations on faults often indicate along-strike variations in displacement and slip rate (Hergert and Heidbach, 2010; Roberts, 2007; Sieh, 1978; Tapponnier et al., 2001). Isolated normal faults typically display symmetrical triangular, elliptical or bell-shaped profiles whereby displacement (and slip rate) increase towards the center of the fault from near zero at the fault tips (Cowie and Scholz, 1992; Kim and Sanderson, 2005; Manighetti et al., 2005; Manzocchi et al., 2006). Deviations from a symmetrical profile may occur due to

*Corresponding author: constanza.rodriguezpiceda@plymouth.ac.uk

multiple factors, including: interactions with adjacent faults (Gupta and Scholz, 2000; Nicol et al., 1996; Peacock and Sanderson, 1991), lateral variations in off-fault damage (Cappa et al., 2014; Perrin et al., 2016), fault bends along the strike (Faure Walker et al., 2009; Iezzi et al., 2018) or downdip linkage with pre-existing structures (Nixon et al., 2014; Phillips et al., 2016). Within active fault systems, detailed information on the spatial variability of slip rate for individual faults remains limited due to incomplete geological and paleoseismological records (Gerstenberger et al., 2020). Therefore, to undertake SHA, it is common to either use a mean or maximum slip rate value collected from the field, or to fit a triangular slip profile through available data (e.g., Chartier et al., 2017; Valentini et al., 2017).

An increasing body of work has highlighted the importance of slip rate spatial variability on earthquake timing and magnitude (Cowie et al., 2012; Delogkos et al., 2023; Faure Walker et al., 2009; Wang and Barbot, 2024; Faure Walker et al., 2018; Perez-Silva et al., 2022). Indeed, Faure Walker et al. (2018) demonstrated that when undertaking fault-based SHA, the consideration of lateral variations in long-term slip rate across faults in the Italian Apennines can affect the calculated recurrence rates and ground-shaking. However, fault-based seismic hazard assessments use empirical relationships (Wells and Coppersmith, 1994; Field et al., 1999) and therefore do not fully capture the physics governing fault slip during the earthquake cycle. Specifically, fault-based SHA neglects the possibility of aseismic slip (i.e., slow slip events, 1e-6 – 1e-4 m/s), releasing a portion of the accumulated geologic moment, and influencing the timing, rupture extent and size of future earthquakes (e.g., Mildon et al., 2024). Aseismic slip can accommodate a significant fraction of the tectonic strain, with estimates ranging from ~10% to 85% depending on the fault and tectonic setting (Avouac, 2015).

Physics-based SHA, based on earthquake cycle simulations, may serve as a complement to fault-based SHA (Milner et al., 2021; Niroula et al., 2025; Rafiei et al., 2022; Shaw et al., 2018; Herrero-Barbero et al., 2023) and can be used to explore how spatially-variable slip rate profiles influence earthquake behavior. Physics-based SHA incorporates the physical processes of earthquake rupture and laboratory-based constraints on the frictional resistance of the fault to generate synthetic seismic catalogs. Earthquake cycle simulators offer several advantages over fault-based SHA. First, they can simulate multiple seismic cycles (>10), addressing the incomplete earthquake record available from geological and geophysical data. Second, they enable controlled numerical experiments by adjusting model input parameters, including long-term slip rate (Delogkos et al., 2023). Seismicity rates and magnitude-frequency distributions (MFDs) extracted from synthetic catalogs can be combined with empirical ground motion prediction equations to estimate earthquake hazard. Similar to fault-based SHA, these simulations often either assume a single value of long-term slip rate or make use of a hybrid loading approach that retains a constant slip rate while tapering stress near fault edges to smooth stress concentrations (Milner et al., 2021; Shaw, 2019); thus, the effect of variable slip distributions in synthetic seismic catalogs from physics-based SHA remains unclear.

In this study, we aim to investigate how spatially variable long-term (Holocene) slip rates measured in the field influence earthquake cycle characteristics (including recurrence times, magnitude-frequency distribution, slip behavior and rupture extent) and associated seismic hazard. First, we numerically simulated earthquake cycles on a 2D normal fault embedded in a 3D elastic medium with the software QDYN (Luo et al., 2017), based on the Parasano-Pescina fault in the Italian Central Apennines (Figure 1). This seismically active region provides well-documented Holocene (15 ± 3 ka) spatially-variable throw rates and derived slip rates (Faure Walker et al., 2021), making it an ideal example to study the effects of spatially variable slip rate on the earthquake cycle. Our tested scenarios range from slip rate profiles considering the complete dataset to simplified profiles often assumed in fault- and physics-based SHA. Second, the resulting earthquake rates and magnitude-frequency distribution from each scenario were combined with empirical ground motion equations to estimate related ground-shaking for specific sites (Bindi et al., 2011). By computing synthetic earthquake catalogues and associated hazards based on models with a rate-and-state friction framework (Dieterich, 1979; Marone, 1998; Ruina, 1983), we are able to capture a broad range of slip modes and thus to analyze the effects on rupture dynamics in the seismicity rates and magnitudes. We show that the choice of slip rate profile and maximum value influences seismic sequences and associated hazard calculations. This implies that the geologic moment rate and the choice of a single long-term slip rate value might be insufficient to characterize the earthquake potential of faults, calling into question some underlying assumptions in traditional fault- and physics-based SHA.

2 Methods

2.1 Earthquake cycle modelling

We used the boundary-element method code QDYN (Luo et al., 2017) to simulate earthquake cycles on a 2D planar normal fault governed by rate-and-state friction and embedded in a 3D elastic medium. The slip behavior of a fault is controlled by the dependency of steady-state friction on the slip velocity. Generally, velocity-strengthening materials (VS), where friction increases with increased velocity, display stable aseismic sliding; whereas velocity-weakening regions (VW), where friction decreases with increasing slip rate, are conditionally stable and can produce earthquake nucleation and rupture propagation (for details on the governing equations and frictional parameters, see Text S1 and Table S1). The shear stress on a fault element relates to its friction coefficient μ and slip rate V via the quasi-dynamic equilibrium equation:

$$\tau_0 + \tau_e - \frac{G}{2c}V = \sigma\mu \tag{2}$$

where τ_0 is the initial shear stress, τ_e is the elastic shear

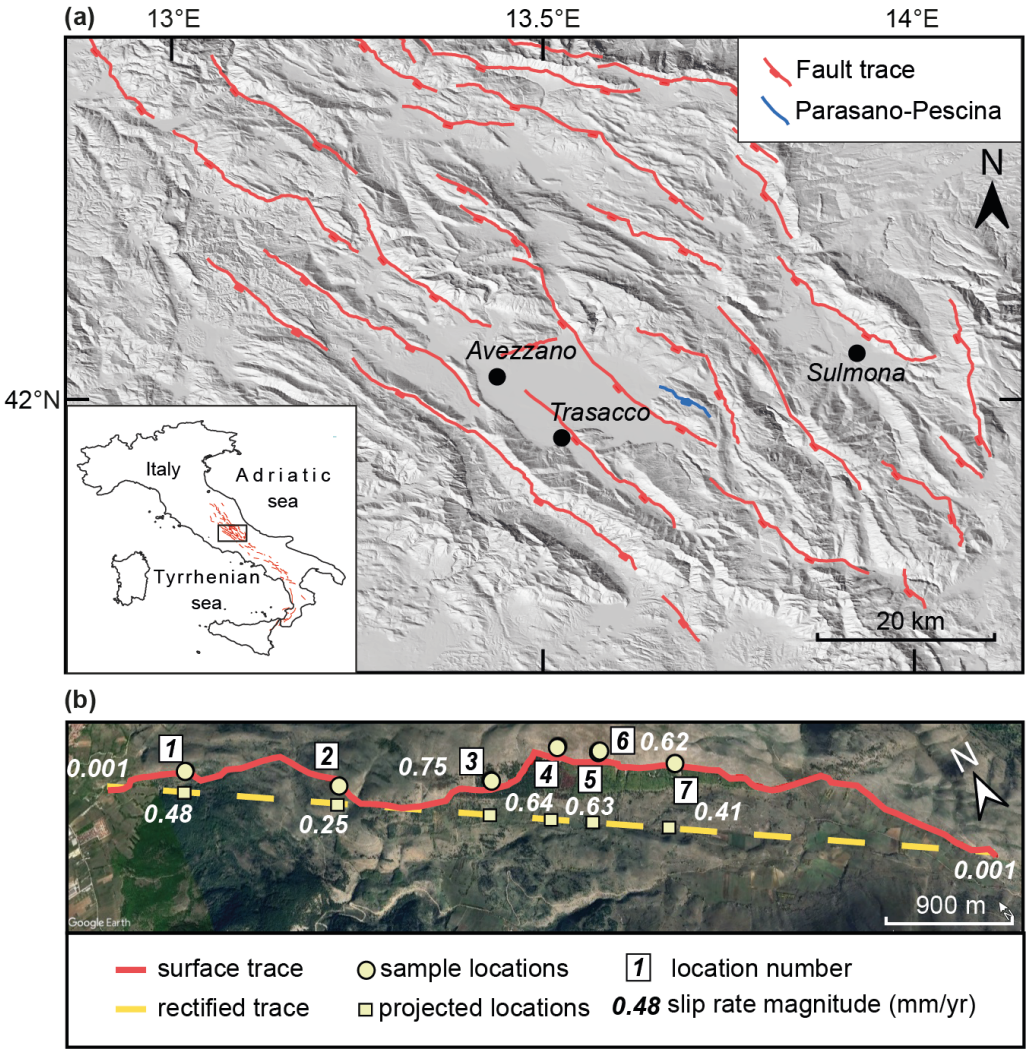

Figure 1 **(a)** Topography of the study area in the Central Apennines taken from TinItaly (Tarquini et al., 2007, 2023) showing surface main traces of active Holocene faults taken from the Fault2SHA database (Faure Walker et al., 2021) and location of sites used for hazard calculations (black markers; see Methods section). **(b)** Surface and rectified traces of the Parasano-Pescina fault with the sample locations and Holocene slip rates (Faure Walker et al., 2021). Note that Holocene slip rate is considered to equal 0.001 mm/yr at the tip of the mapped surface trace to mimic the natural tapering of slip (Imagery data: Google Earth, 2024 Airbus).

stress due to slip, σ is the normal stress and $\frac{G}{2c}V$ is the radiation damping term with c being the seismic S-wave velocity. QDYN utilizes the backslip approach, in which fault elements exert stresses onto the other elements that are proportional to their slip deficit relative to the long-term slip rate V_g (Heimisson, 2020; Savage, 1983). In this interpretation of backslip, faults are approximately modelled as faults of finite size remotely loaded by tectonics stresses (Allam et al., 2019; Dieterich and Smith, 2009). This method is able to approximately account for off-fault inelastic deformation, which relaxes accumulated stresses due to increasing slip, stresses that would otherwise continue to build indefinitely. It achieves this while maintaining the target fault long-term slip rate.

The elastic shear stress τ_i^e on the i-th fault element is the sum of shear stress contributions of all the surrounding fault elements:

$$\tau_i^e = -\sum_j k_{ij}^\tau \left(u_j(t) - V_g t\right) \qquad (3)$$

where u_j is the slip on the j-th element and k_{ij}^τ is the stiffness matrix for shear stress, which represents the stress on the i-th element produced by a unit of slip in the j-th element. An equivalent relationship to eq. 3 exists for the normal stress. To accelerate the computations, the along-strike interactions are computed as spatial convolutions in the spectral domain using the Fast Fourier Transform, thus the fault geometry is a planar surface of constant strike. To accommodate these geometrical restrictions, we simplified the mapped surface fault trace to a 7-km-long linear trace using the smoothing Douglas-Peucker algorithm in QGIS (QGIS Development Q.G.I.S.Development Team, 2009). The fault plane was then created by extending the fault trace to depth by taking the average fault dip measured in the field (60.4°, Faure Walker et al., 2021), and meshing the surface downdip to 15 km depth (Fig. 2a). This depth coincides with the inferred brittle-ductile transition of faults in the area, based on earthquake locations (Chiaraluce et al., 2022) and heat flow measurements (Cowie et al., 2013). The across-strike and down-dip grid sizes (Dx and

Dw) were set to properly resolve the rupture nucleation and propagation processes (Supplementary Text S1).

We considered a rectangular asperity of velocity weakening properties, surrounded by a ~200 m wide area of velocity strengthening material to prevent strong stress concentration along the asperity rim due to the backslip approach (Fig. 2a). The aspect ratio of the asperity is within the range encountered for natural examples of normal faults (Nicol et al., 1996). Our study is focused on the effect of variable loading velocity in the seismic sequence; thus, we do not impose any other frictional heterogeneity on the asperity, but we expect complexities in the seismic sequence to emerge solely from the heterogeneous long-term slip velocity. Among the uniform rate-and-state friction parameters, the chosen (a-b) is consistent with laboratory experiments on carbonate-rich gouges (e.g., Chen and Spiers, 2016) and is characteristic of a fault with weak velocity-weakening behavior (a/b ratio=0.5). To determine the robustness of the results, we perform a sensitivity analysis with lower a/b ratios (i.e. more velocity-weakening, Table S3), and investigated their impact on earthquake magnitude and recurrence distributions under the same loading conditions.

To study the impact of spatial variability in slip rate profiles, we created 16 model set-ups using realistic interpolation strategies from field data. These generally involve line segments connecting or enveloping discrete field slip rate data, by either assuming boxcar, triangular or elliptical shapes (Manighetti et al., 2001; Nicol et al., 1996). For all models, we assumed that the slip rate at the end of the fault is 0.001 mm/yr, consistent with geological observations at fault tips (Manighetti et al., 2005; Nicol et al., 1996). A reference model ("all data linear") captures the measured spatial heterogeneity in long-term slip rate by performing a linear interpolation of all available slip rate measurements for the Parasano-Pescina fault (Fig. 1a). We created alternative slip rate profiles by either applying a spline interpolation ("all data spline"), or by assuming degraded-data profiles with a triangular, elliptical or boxcar shape: "triangular max", "triangular mean", "triangular min", "triangular left", "triangular right", "boxcar max", "boxcar mean", "boxcar min", "elliptical max", "elliptical mean" and "elliptical min" (Figs 3 and S1). These scenarios were designed to represent a broad spectrum of potential values that could arise when the average slip rate is derived from fewer measurements. The slip rate profile for each model set-up was then projected onto a planar fault geometry. In the absence of robust constraints about the slip rate distribution in depth, surface slip rate values were extended uniformly downdip, an approach also adopted by other modelling studies in the region (e.g., Mildon et al., 2022; Wedmore et al., 2017). However, based on single-event slip distributions and observed depth variations of seismicity rates, it has been suggested that long-term slip rates vary with depth, typically tapering near the surface and the base of the seismogenic zone, with a maximum at intermediate depths (Delogkos et al., 2023; Finocchio et al., 2016; Ragon et al., 2019; Scognamiglio et al., 2018). We then tested two alternative scenarios, based on the "All-data" and "Triangular max" profiles, by introducing downdip variations in slip rate. In these models, slip rate peaks at depth at twice the surface value, tapering upward to match the field-based measurements and downward to 0.001 mm/yr at the base of the fault.

We ran the simulations for 100,000 years to ensure enough seismic events were captured for the comparison of catalogues between slip rate profiles, and so that the initial spin up cycles (2,500 years) could be discarded. A seismic event is defined as ongoing if at least one fault element is slipping faster than 0.01 m/s.

We investigated how lateral variations in the magnitude of long-term slip velocity affect the periodicity of the earthquake cycle on faults by looking at two metrics: the distribution of recurrence time of all seismic events (T_r) and the coefficient of variation of these recurrence times on the fault (CV, $CV = \frac{T_{r\ std}}{T_{r\ mean}}$). The latter describes the degree of aperiodicity of the distribution of recurrence times: CV ~0 indicates a periodic seismic cycle; CV=1 indicates a random Poissonian distribution of the recurrence times, and CV>1 indicates that the seismic events are clustered (Boschi et al., 1995).

2.2 Seismic hazard calculations

We investigated the impact of varying long-term slip rates on the seismic hazard associated with the Parasano-Pescina fault by computing hazard curves, which represent the annual probability of exceeding a specific peak ground acceleration (PGA) at specific sites. For each of the modelled slip rate configurations, we used the earthquake rates and magnitude-frequency distributions to estimate the probability of exceedance (PoE) of different PGA levels. The nearby town of Trasacco, located ~12km to the south-west of the Parasano-Pescina fault (Fig. 1) was used as the reference site due to its proximity to the fault trace. Additional calculations were done for the more distant sites of Avezzano and Sulmona (Fig. 1a). We adopted an empirical ground motion model (GMM) specifically calibrated with strong-motion data from Italy (Bindi et al., 2011) (see Supplementary Text S3).

3 Results

In the following section, we refer to supplementary videos that can be found in a dedicated repository (Rodriguez Piceda, 2025), alongside other data and scripts generated in this study. For brevity, we refer to this repository as "RP25" in the relevant places below

3.1 Characteristics of earthquake cycles

The shape of the long-term slip rate profile was found to cause variations in the synthetic earthquake catalogs (Fig. 3). Full-data models ("All data linear" and "All data spline") show the largest variations in the earthquake nucleation location, slip behavior, and rupture length (Fig. 3a-b). The rupture extent is heterogeneous, with the emergence of full and partial ruptures. Seismic events are characterized by a phase of aseismic slip in the regions of the first and second long-term slip

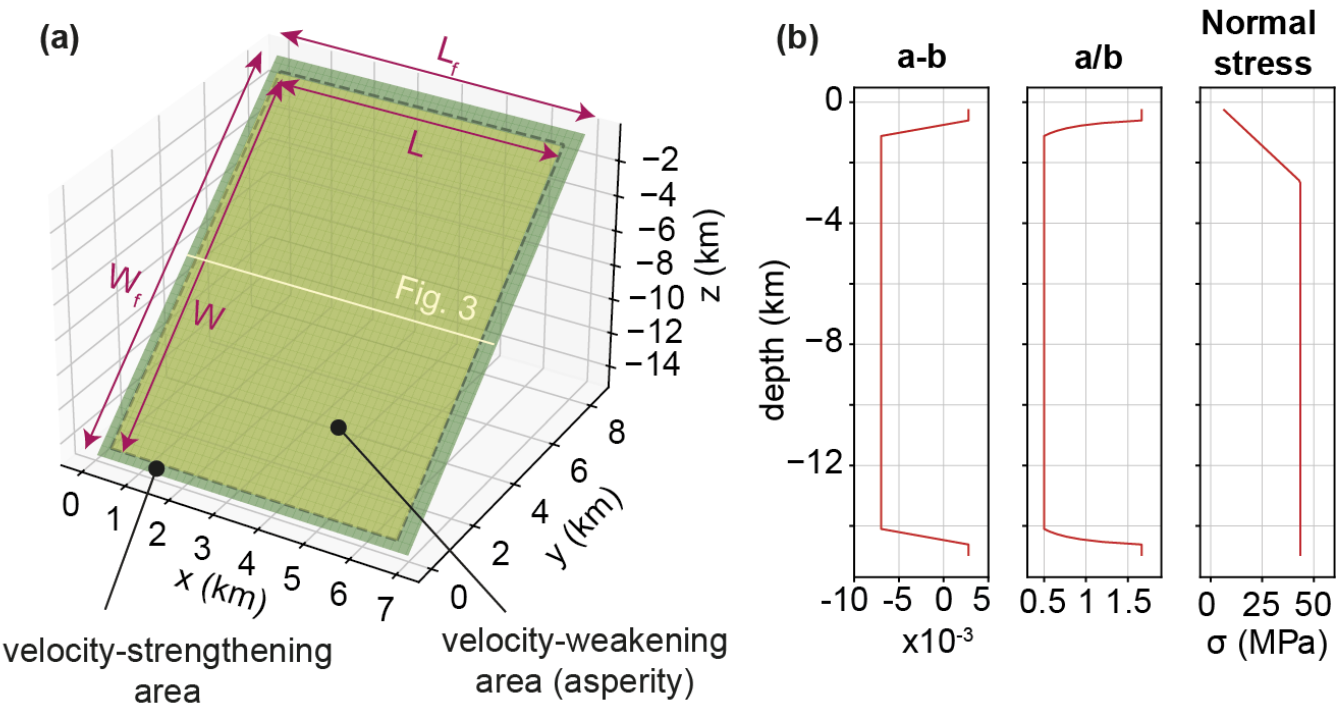

Figure 2 **(a)** 3D visualization of the model set-up for the Parasano-Pescina fault. The lighter-colored area is velocity-weakening, while the darker-colored area is velocity-strengthening. L_f and W_f are length and width of the fault, respectively. L and W are length and width of the velocity-weakening region or asperity, respectively. **(b)** Depth profiles showing the distribution of frictional parameters a, b and normal stress (for details see Supplementary Text S1 and S2).

rate maxima. This is followed by a rupture nucleating towards the center of the fault, coinciding either with the long-term slip rate maximum or second maximum. Ruptures grow first down-dip until saturating the fault width and then bilaterally (Videos S1-S2, RP25). The regions of slow long-term slip rate act as barriers to the rupture propagation, slowing down the rupture or even provoking its arrest. In the interseismic periods, slow slip events with slip rates of 1e-7 to 1e-6 m/s are observed (Fig. 3a-b, Videos S1-S2, RP25). Unlike the "All data -linear" model, the "All data – spline" model is characterized by the generation of earthquake doublets, with one seismic event nucleating in the middle of the fault partially rupturing the fault, followed by a second event nucleating towards the left side of the fault. The second event ruptured the region that was not ruptured during the initial event (Fig. 3b; Video S2, RP25). Therefore, even when all datapoints are taken into consideration, the interpolation methodology can influence the resulting synthetic catalogue.

For the simplified long-term slip rate profiles, the nucleation and propagation of events is less complex than for the all-data models (Fig. 3c-e; S1; Videos S3-S13, RP25). Events always nucleate in the region of maximum slip rate and grow first bilaterally and then downdip. Models with asymmetrical triangular profiles alternate between full and partial ruptures (Fig. S1f-g; Videos S9-S10, RP25), while only full ruptures are generated in the models with symmetric-triangular, boxcar and elliptical profiles (Fig. S1a-d, g-h; Videos S3-S8, S11-S13, RP25).

Magnitude-frequency distributions differ between models, with the "All data – linear" model generating the widest range of M_w from 4.5 to 6.2, and most events exceeding M_w 5.75 (Fig. 4a). The "All data – spline" model is associated with a bimodal distribution of events between 5.9 and 6.2, representative of the earthquake doublets. In contrast, models with a simplified slip rate profile show a characteristic M_w of 6.2, with only the model "Triangular left" showing also seismic events with M_w of 5.9.

More complex slip rate profiles produce larger variability of T_r, and thus higher CV than simplified profiles (Fig. 4b). In the "All data linear" model, recurrence times vary from ~0 yr to 3,500 yr with average of ~2,800 yr. A larger number of seismic events with T_r~0 appears in model "All data-spline" compared to "All data-linear", corresponding to the recurrence times between seismic events of an earthquake doublet. Consequently, the CV of the "All data-spline" model is higher than the CV of the "All data-linear" model (0.65 vs 0.25), which correspond with less and more periodic seismic cycles, respectively. The models with simplified slip rate profiles have a narrower range of T_r, in most cases a unique value, which translates to a lower CV (~0 to 0.08), indicative of a periodic cycle. For the same profile shape, T_r increases with decreasing slip rate. Smaller or larger long-term slip rate magnitudes imply that the fault is loaded more slowly or rapidly, respectively, resulting in longer or shorter recurrence times (Fig. 4b).

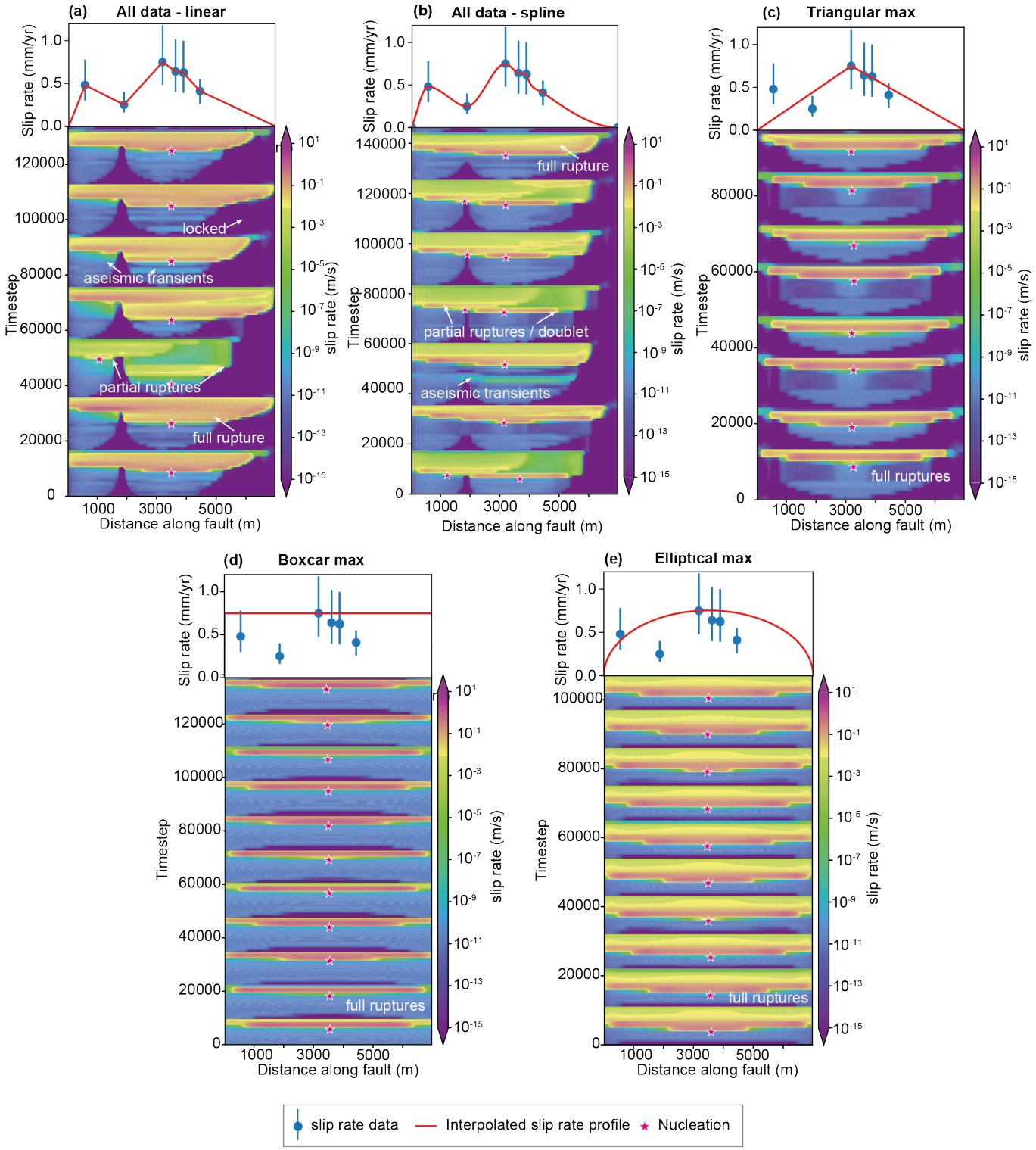

Figure 3 Slip rate evolution of models "All data-linear", "Triangular max", "Boxcar max" and "Elliptical max". Top subpanels: Long-term slip rate profiles used in the simulation, based on the seven field slip rate measurements (blue symbols) along the Parasano-Pescina fault (Faure Walker et al., 2021). In all the models, the long-term slip rate is tapered to 0.001 mm/yr at the edges of the fault to mimic the natural tapering of slip. Bottom panels: Evolution of the slip rate along a horizontal profile taken at a depth of 7.5 km (Fig. 2a) between 20,000 and 40,000 years. Note that, due to QDYN's adaptive time-stepping, in the co-seismic period timesteps are smaller than in the inter-seismic period. **(a)** "all data linear" uses a linear interpolation between all the data; **(b)** "all data spline" uses a monotonic cubic spline interpolation between all the data; **(c)** "triangular max" uses the maximum value of slip rate and this decreases linearly from the maximum to 0.001 mm/yr at each tip; **(d)** "boxcar max" uses only the maximum value of slip rate; **(e)** "elliptical max" uses a semielliptical interpolation between the maximum value of slip rate and 0.001 mm/yr in the fault tips. Magenta stars show the nucleation location of events. The model with detailed slip rate profile produces a wider range of rupture lengths and slip modes compared to simplified profiles.

The sensitivity analysis of the effect of rate-and-state frictional parameters on the seismic behavior yields consistent patterns across all tested a/b ratios (Figs S3-S7). In each set of models with different long-term slip rate profiles, those with the "All-data" slip rate profiles show broader magnitude frequency distributions and higher coefficients of variation in recurrence intervals compared to the simplified slip rate profiles. Among the simplified slip rate cases, triangular profiles most closely reproduce the behavior of the "All-data" models. Notably, in models with lower a/b ratios (i.e., more velocity-weakening) the differences in the seismicity magnitude and recurrence decreases across models with different slip rate profiles. In these models, the resulting magnitude-frequency and recurrence distributions show less sensitivity to the imposed long-term slip rate distributions, yielding more consistent behaviors across slip rate scenarios compared to the reference model set (Fig. 4).

In simulations that include downdip variations in long-term slip rate, earthquake magnitude and recurrence intervals show narrower variability compared to their counterparts with uniform downdip slip rate distributions (Fig. S8). For the "All-data" case, magnitudes range between 6.1 and 6.2, while for the "Triangular max" case, they range between 6 and 6.2. Recurrence intervals are also more regular in the downdip tapered models, but their absolute values still differ from those in models with more uniform slip rate distributions (e.g., the "boxcar" case).

3.2 Seismic hazard curves

Figure 5a shows the annual PoE for different PGA values at the site Trasacco, while results for the sites Avezanno and Sulmona are shown in Fig. S3. The PoE varies across models (Fig. 5a). For a PGA of 0.25 g, simulations using slip rate profiles centered around the minimum datapoint ("Triangular min", "Boxcar min", and "Elliptical min") show a lower PoE (7e-5 - 1e-4) compared to the "All data – linear" model (11e-4) due to their longer predicted recurrence times. In contrast, models with slip rate profiles centered around the maximum datapoint ("Triangular max", "Boxcar max", and "Elliptical max") produce a higher PoE (4 - 5.5e-4) for the same PGA, which can be attributed to their shorter recurrence times compared to the 'All data – linear" model.

When comparing models with the same central datapoint but different slip rate profile shapes, PoE is the lowest for the "Triangular" model, and is the highest for the "Boxcar" and "Elliptical" model, reflecting progressively shorter recurrence times, though these differences are minor. Among the simplified slip rate profile models, "Triangular left", "Triangular max", and the models centered in the mean most closely resemble the reference model curve. Lastly, among models where all datapoints are taken into consideration, the "All data - spline" shows a higher PoE than the "All data – linear" model for PGAs smaller than 0.5, likely due to the shorter recurrence times of the former, which shows that the choice of interpolation method also influences the predicted hazard. For the more distant sites of Avezzano and Sulmona (Fig. S9), the comparison between models remains consistent with that of Trasacco, although the PoE values are lower due to the larger distance from the Parasano-Pescina fault.

4 Discussion

One key point of discussion is whether physics-based SHA is more or less sensitive to the choice of slip rate profile compared to fault-based SHA (e.g., Faure Walker et al., 2018). In fault-based SHA, long-term slip rates are typically used to derive earthquake rates (Chartier et al., 2019; Pace et al., 2016; Tavakolizadeh et al., 2024; Faure Walker et al., 2018). For instance, in the fault-based SHA study by Faure Walker et al. (2018), slip rates impact the calculation of recurrence times through the "segment seismic moment conservation" criterion (Field et al., 1999). On the other hand, the range of possible magnitudes typically follows a truncated Gutenberg-Richter distribution with maximum magnitudes derived from fault-length scaling relationships (Wells and Coppersmith, 1994). Therefore, magnitude-frequency distributions are not directly affected by the choice of slip rate profile in fault-based assessments, as it does for physics-based assessments.

According to the "segment seismic moment conservation" criterion (Field et al., 1999), the entire accumulated geologic moment, as determined by a long-term slip rate, is released through earthquakes. This implies that the mean recurrence time T_{Mmax} for full-rupture events with a maximum possible magnitude $M_{\max}$ is inversely proportional to the geologic moment accumulation rate $\dot{M}_g$ determined by the long-term slip rate V_g (Pace et al., 2016):

$$T_{Mmax} = \frac{10^{1.5M_{\max}+9.1}}{\dot{M}_g} \tag{4}$$

For faults with variable slip rate along-strike, the calculation of $\dot{M}_g$ can be generalized as:

$$\dot{M}_g = G \sum L_i W_i V_{gi} \tag{5}$$

Where V_{gi} is the slip rate data of the along-strike fault segment with length L_i and width W_i. We compared the mean recurrence times of full-rupture events ($M_w \geq 6.1$) from our models with the mean recurrence times predicted by eqs 4 – 5, which assumes that all geological moment is converted to seismic moment (Fig. 5b). The modelled data show dispersion and does not align well with the recurrence times predicted by eqs 1 and 5. This large dispersion indicates that $\dot{M}_g$ might not be sufficient to characterize the expected recurrence times, and that the spatial distribution of slip rate (i.e., the shape of the curve) also plays an important role. While a general decrease in T_{Mmax} with increasing moment rate is observed, our models produce T_{Mmax} larger than the T_{Mmax} estimated by 5. This discrepancy suggests that a significant portion of the tectonic strain is being released through mechanisms other than full-rupture events, such as partial ruptures, steady creep or

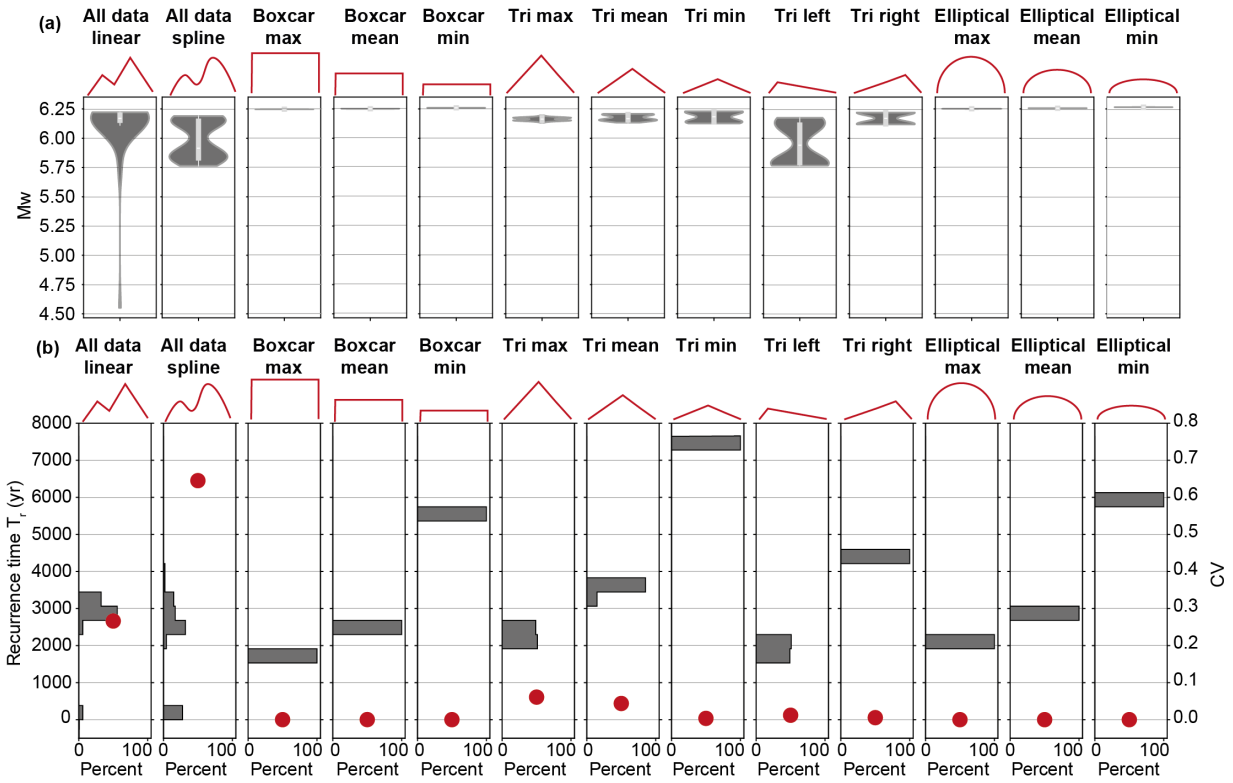

Figure 4 **(a)** Magnitude-frequency distribution shown as kernel-density functions. More complex slip rate profiles generate a wider range of magnitudes than simplified profiles; **(b)** Coefficient of variation (CV, red dots) and histogram of recurrence time (Tr, grey bars) for each simulation. More complex slip rate profiles produce a larger variability of Tr, and thus higher CV than simplified profiles. For the same profile shape, Tr increases with decreasing slip rate. For descriptions of the slip rate profiles, see 3.

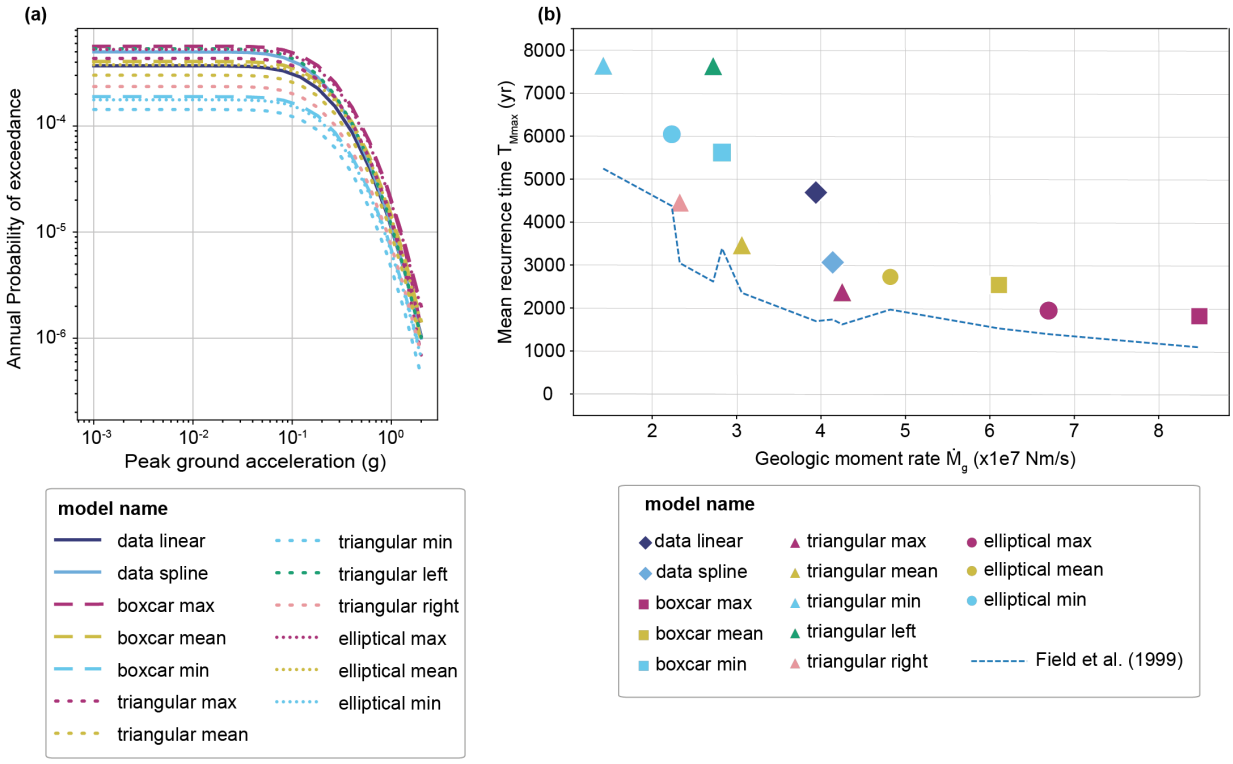

Figure 5 **(a)** Hazard curves of annual probability of exceedance for a given peak ground acceleration for the Parasano-Pescina fault at Trasacco (for site location relative to the fault trace, see Fig. 1 and S1); **(b)** Comparison between mean recurrence time T_{Mmax} of full-rupture seismic events (M_w>6.1) obtained from Field et al. (1999) segment seismic moment conservation equation (4 – 5; dashed blue line) and T_{Mmax} from models with different slip rate profiles (markers) vs. geologic moment rate.

episodes of aseismic slip. These factors ultimately affect the timing of full-rupture events and suggests that recurrence times, and by extension, seismic hazard estimates, derived from physics-based SHA are more sensitive to the choice of slip rate profiles than those obtained from fault-based SHA (i.e. based on eqs 4 – 5). Consequently, with earthquake simulators becoming increasingly popular for SHA (Gerstenberger et al., 2024; Niroula et al., 2025; Shaw et al., 2018; Milner et al., 2021), it is important to evaluate the uncertainties associated with selecting a long-term slip rate profile for a fault, especially when multiple slip rate measurements are available.

Our results show that spatially heterogeneous slip rate profiles greatly affect the seismic cycle on faults, including nucleation location, slip modes, earthquake magnitude and recurrence times (Figs 3 – 5). Due to the spatial variability in slip rate, the fault accumulates stress at different rates, leading to a heterogenous stress distribution across the fault surface at a given time. Stress heterogeneities create conditions for the emergence of partial ruptures and/or episodes of slow slip, where the rupture is unable to propagate beyond areas of slip rate minima. Partial ruptures add to the variability in the stress distribution, generating a feedback effect which promotes partial ruptures and additional episodes of slow slip. This ultimately affects earthquake recurrence times and magnitude-frequency distributions. Consequently, synthetic earthquake catalogues generated using spatially heterogeneous slip rate profiles are more likely to generate magnitude distributions that resemble more closely a Gutenberg-Richter relationship rather than a characteristic earthquake scaling. This result aligns closely with those of Delogkos et al. (2023) with their model with along-strike and down-dip variations in slip rates. Due to the less restrictive assumptions of our modelling approach, we also find additional complexities in our simulations, such as the emergence of aseismic slip transients.

The sensitivity analysis on frictional parameters shows that more-velocity weakening faults, characterized by lower a/b ratios, produce earthquake sequences that are less influenced by the choice of long-term slip rate profiles. Although some differences persist, recurrence intervals and magnitude-frequency distributions are more similar across slip rate scenarios. In these models, rupture nucleation and propagation are primarily controlled by the strength of the attractor of the frictional limit cycle than to the spatial pattern of loading (Barbot, 2019; Cattania, 2019). In other words, when a/b is lower than 0.5, the system exhibits a more stable limit cycle, and is less affected by external loading heterogeneities.

The present study focuses on slip rate variability and its impact on seismic hazard on a single fault. Faults, however, do not appear in isolation but are embedded within fault networks where stress interactions strongly influence their slip behavior. Observations on relay ramps, overlapping fault segments and stepovers indicate that, as slip decreases on one fault, it commonly increases on a nearby faults (Cartwright et al., 1995; Manighetti et al., 2001; Peacock and Sanderson, 1991). This complementary pattern suggests that slip rate variability and its influence on seismic hazard may differ depending on whether faults are considered individually or collectively as a system. Future work could test the impact of spatially variable slip rates by comparing isolated faults with fault networks.

In natural fault systems, it is challenging to accurately measure two or three dimensional variations in slip rate, often forcing SHA to rely on simplified slip rate profiles (Shaw et al., 2018; Valentini et al., 2017; Williams et al., 2023; Gómez-Novell et al., 2020; Herrero-Barbero et al., 2023). Therefore, a relevant point for SHA is to determine the necessary spatial resolution for slip rate data needed to resolve along-strike profiles sufficiently to ensure that further measurements do not impact the inferred recurrence times, maximum M_w and associated hazard estimates. Our results show that multiple degraded-data profiles produce mean recurrence times similar to those of the "All-data" profiles (e.g. "Triangular max", "triangular mean", "Triangular left" and "Elliptical mean"), albeit with less dispersion. Despite this, some cases of degraded profiles tend to overestimate the PGAs with respect to the "All-data" cases, while some others tend to underestimate it. This is likely caused by the differences in mean recurrence times. From all the tested configurations, using a simplified slip rate distribution with a "Triangular left", "Triangular max" or a model centered in the mean appears to be the closest approximation in terms of produced PGAs to the "All-data" profile. The elliptical profile shape aligns with observed slip distributions on earthquake ruptures (Cappa et al., 2014). To assess whether this finding can be applied to other faults, a similar approach should be tested on other well-studied faults with ample slip rate data.

In this study, we undertook a simplified SHA approach using a single simplified fault geometry and an empirical GMM. To derive more extensive conclusions, a full PSHA involving the use of multiple fault geometries and GMMs and magnitude through a logic tree approach to evaluate epistemic uncertainties should be undertaken (Faure Walker et al., 2019). However, it is clear that uncertainties introduced by considering degraded-data profiles would be larger for faults where complex spatial variations of slip rate are expected, as is the case for faults with multiple structures across strike (Gupta and Scholz, 2000; Nicol et al., 1996; Peacock and Sanderson, 1991), bends (Delogkos et al., 2020; Iezzi et al., 2018), and off-fault deformation (Perrin et al., 2016). In such cases, fault geometry itself can influence where and how slip accumulates over time (Allam et al., 2019; Faure Walker et al., 2018). Although geometric irregularities can produce spatial variability in coseismic slip under uniform loading (Allam et al., 2019), this does not necessarily imply equivalent variability in long-term slip rate, which reflects the averaged behavior over multiple cycles. Still, geometry and long-term slip rate are not fully independent and should ideally be considered together in SHA. Spatial slip rate variability may also influence rupture directivity by promoting preferential rupture directions, reinforcing the need to incorporate directivity effects into GMMs when

assessing these faults. Overall, it is expected that faults that share some of these characteristics would require a higher sampling resolution compared to those that do not. Where this is not possible, SHA should incorporate simulations across a range of geologically realistic profiles.

Models with downdip variations in long-term slip rate tend to produce more regular earthquake recurrence and characteristic magnitudes than those loaded with uniform slip rate in depth. This is likely because the tapering towards the surface and the bottom of the fault reduces strong lateral gradients in slip rate at those depths, thus lateral propagation is less likely to be arrested, which ultimately promotes full ruptures with characteristic magnitudes. In these models, events also tend to nucleate at intermediate depths (e.g. Videos S14-S15, RP25), where the prescribed long-term slip rate peaks, which aligns with observations from single-event slip distributions and depth-dependent seismicity rates (Delogkos et al., 2023; Finocchio et al., 2016; Ragon et al., 2019; Scognamiglio et al., 2018). However, it is worth noting that models with uniform downdip loading but variable along-strike loading can also show depth-variable nucleation, with events nucleating at intermediate depths (e.g. Videos S14-S15, RP25). This suggests that a variable downdip slip rate is not strictly necessary to reproduce the observed downdip patterns of seismicity and slip.

Overall, our study and previous work demonstrates that considering spatially heterogeneous slip rates introduces larger variabilities in slip modes, seismicity rates, magnitude frequency distributions than simplified fault slip rate profiles, thus impacting hazard calculations. Therefore, we argue that detailed fault-slip rate profiles are needed, especially when undertaking physics-based assessments on faults with complex slip geometries.

Acknowledgements

This research was funded by UK Research and Innovation (UKRI) under the auspices of the project Quake4D (MR/T041994/1) awarded to Zoë Mildon. This work was carried out using the ARCHER2 UK National Supercomputing Service (https://www.archer2.ac.uk). We thank Octavi Gómez Novell and an anonymous reviewer for their comments which helped to improve this manuscript. We are also grateful to the editor Alexandra Hatem and the Seismica team for their handling of the review and copyediting process.

5 Data and code availability

QDYN is open source (Luo et al., 2017). The simulations were run with the QDYN version release 3.0.0. The input files to reproduce the results, scripts to plot the figures of this work and videos of model simulations are available at Rodriguez Piceda (2025).

6 Competing interests

The authors have no competing interests.

References

Allam, A. A., Kroll, K. A., Milliner, C. W. D., and Richards-Dinger, K. B. Effects of Fault Roughness on Coseismic Slip and Earthquake Locations. *Journal of Geophysical Research: Solid Earth*, 124 (11):11336–11349, Nov. 2019. doi: 10.1029/2018jb016216.

Avouac, J.-P. From Geodetic Imaging of Seismic and Aseismic Fault Slip to Dynamic Modeling of the Seismic Cycle. *Annual Review of Earth and Planetary Sciences*, 43(1):233–271, May 2015. doi: 10.1146/annurev-earth-060614-105302.

Barbot, S. Slow-slip, slow earthquakes, period-two cycles, full and partial ruptures, and deterministic chaos in a single asperity fault. *Tectonophysics*, 768:228171, Oct. 2019. doi: 10.1016/j.tecto.2019.228171.

Bindi, D., Pacor, F., Luzi, L., Puglia, R., Massa, M., Ameri, G., and Paolucci, R. Ground motion prediction equations derived from the Italian strong motion database. *Bulletin of Earthquake Engineering*, 9(6):1899–1920, Sept. 2011. doi: 10.1007/s10518-011-9313-z.

Boschi, E., Gasperini, P., and Mulargia, F. Forecasting where larger crustal earthquakes are likely to occur in Italy in the near future. *Bulletin of the Seismological Society of America*, 85(5): 1475–1482, 10 1995. doi: 10.1785/BSSA0850051475.

Brune, J. N. Seismic moment, seismicity, and rate of slip along major fault zones. *Journal of Geophysical Research*, 73(2):777–784, Jan. 1968. doi: 10.1029/jb073i002p00777.

Cappa, F., Perrin, C., Manighetti, I., and Delor, E. Off-fault long-term damage: A condition to account for generic, triangular earthquake slip profiles. *Geochemistry, Geophysics, Geosystems*, 15 (4):1476–1493, Apr. 2014. doi: 10.1002/2013gc005182.

Cartwright, J. A., Trudgill, B. D., and Mansfield, C. S. Fault growth by segment linkage: an explanation for scatter in maximum displacement and trace length data from the Canyonlands Grabens of SE Utah. *Journal of Structural Geology*, 17(9):1319–1326, Sept. 1995. doi: 10.1016/0191-8141(95)00033-a.

Cattania, C. Complex Earthquake Sequences On Simple Faults. *Geophysical Research Letters*, 46(17–18):10384–10393, Sept. 2019. doi: 10.1029/2019gl083628.

Chartier, T., Scotti, O., Clément, C., Jomard, H., and Baize, S. Transposing an active fault database into a fault-based seismic hazard assessment for nuclear facilities – Part 2: Impact of fault parameter uncertainties on a site-specific PSHA exercise in the Upper Rhine Graben, eastern France. *Natural Hazards and Earth System Sciences*, 17(9):1585–1593, Sept. 2017. doi: 10.5194/nhess-17-1585-2017.

Chartier, T., Scotti, O., and Lyon-Caen, H. SHERIFS: Open-Source Code for Computing Earthquake Rates in Fault Systems and Constructing Hazard Models. *Seismological Research Letters*, May 2019. doi: 10.1785/0220180332.

Chen, J. and Spiers, C. J. Rate and state frictional and healing behavior of carbonate fault gouge explained using microphysical model. *Journal of Geophysical Research: Solid Earth*, 121(12): 8642–8665, Dec. 2016. doi: 10.1002/2016jb013470.

Chiaraluce, L., Michele, M., Waldhauser, F., Tan, Y. J., Herrmann, M., Spallarossa, D., Beroza, G. C., Cattaneo, M., Chiarabba, C., De Gori, P., Di Stefano, R., Ellsworth, W., Main, I., Mancini, S., Margheriti, L., Marzocchi, W., Meier, M.-A., Scafidi, D., Schaff, D., and Segou, M. A comprehensive suite of earthquake catalogues for the 2016-2017 Central Italy seismic sequence. *Scientific Data*, 9(1), Nov. 2022. doi: 10.1038/s41597-022-01827-z.

Cowie, P. A. and Scholz, C. H. Growth of faults by accumulation of seismic slip. *Journal of Geophysical Research: Solid Earth*, 97 (B7):11085–11095, July 1992. doi: 10.1029/92jb00586.

Cowie, P. A., Roberts, G. P., Bull, J. M., and Visini, F. Relationships between fault geometry, slip rate variability and earthquake recurrence in extensional settings. *Geophysical Journal International*, 189(1):143–160, Feb. 2012. doi: 10.1111/j.1365-246x.2012.05378.x.

Cowie, P. A., Scholz, C. H., Roberts, G. P., Faure Walker, J. P., and Steer, P. Viscous roots of active seismogenic faults revealed by geologic slip rate variations. *Nature Geoscience*, 6(12): 1036–1040, Nov. 2013. doi: 10.1038/ngeo1991.

Delogkos, E., Saqab, M. M., Walsh, J. J., Roche, V., and Childs, C. Throw variations and strain partitioning associated with fault-bend folding along normal faults. *Solid Earth*, 11(3):935–945, May 2020. doi: 10.5194/se-11-935-2020.

Delogkos, E., Howell, A., Seebeck, H., Shaw, B. E., Nicol, A., Mika Liao, Y., and Walsh, J. J. Impact of Variable Fault Geometries and Slip Rates on Earthquake Catalogs From Physics-Based Simulations of a Normal Fault. *Journal of Geophysical Research: Solid Earth*, 128(11), Nov. 2023. doi: 10.1029/2023jb026746.

Dieterich, J. H. Modeling of rock friction: 1. Experimental results and constitutive equations. *Journal of Geophysical Research: Solid Earth*, 84(B5):2161–2168, May 1979. doi: 10.1029/jb084ib05p02161.

Dieterich, J. H. and Smith, D. E. *Nonplanar Faults: Mechanics of Slip and Off-fault Damage*, page 1799–1815. Birkhäuser Basel, 2009. doi: 10.1007/978-3-0346-0138-2_12.

Faure Walker, J., Roberts, G., Cowie, P., Papanikolaou, I., Sammonds, P., Michetti, A., and Phillips, R. Horizontal strain-rates and throw-rates across breached relay zones, central Italy: Implications for the preservation of throw deficits at points of normal fault linkage. *Journal of Structural Geology*, 31(10): 1145–1160, Oct. 2009. doi: 10.1016/j.jsg.2009.06.011.

Faure Walker, J., Boncio, P., Pace, B., Roberts, G., Benedetti, L., Scotti, O., Visini, F., and Peruzza, L. Fault2SHA Central Apennines database and structuring active fault data for seismic hazard assessment. *Scientific Data*, 8(1), Mar. 2021. doi: 10.1038/s41597-021-00868-0.

Faure Walker, J. P., Visini, F., Roberts, G., Galasso, C., McCaffrey, K., and Mildon, Z. Variable Fault Geometry Suggests Detailed Fault-Slip-Rate Profiles and Geometries Are Needed for Fault-Based Probabilistic Seismic Hazard Assessment (PSHA). *Bulletin of the Seismological Society of America*, 109(1):110–123, Nov. 2018. doi: 10.1785/0120180137.

Field, E. H., Jackson, D. D., and Dolan, J. F. A mutually consistent seismic-hazard source model for southern California. *Bulletin of the Seismological Society of America*, 89(3):559–578, June 1999. doi: 10.1785/bssa0890030559.

Field, E. H., Arrowsmith, R. J., Biasi, G. P., Bird, P., Dawson, T. E., Felzer, K. R., Jackson, D. D., Johnson, K. M., Jordan, T. H., Madden, C., Michael, A. J., Milner, K. R., Page, M. T., Parsons, T., Powers, P. M., Shaw, B. E., Thatcher, W. R., Weldon, R. J., and Zeng, Y. Uniform California Earthquake Rupture Forecast, Version 3 (UCERF3)–The Time-Independent Model. *Bulletin of the Seismological Society of America*, 104(3):1122–1180, June 2014. doi: 10.1785/0120130164.

Finocchio, D., Barba, S., and Basili, R. Slip rate depth distribution for active faults in Central Italy using numerical models. *Tectonophysics*, 687:232–244, Sept. 2016. doi: 10.1016/j.tecto.2016.07.031.

Gerstenberger, M. C., Marzocchi, W., Allen, T., Pagani, M., Adams, J., Danciu, L., Field, E. H., Fujiwara, H., Luco, N., Ma, K., Meletti, C., and Petersen, M. D. Probabilistic Seismic Hazard Analysis at Regional and National Scales: State of the Art and Future Challenges. *Reviews of Geophysics*, 58(2), June 2020. doi: 10.1029/2019rg000653.

Gerstenberger, M. C., Van Dissen, R., Rollins, C., DiCaprio, C., Thingbaijim, K. K. S., Bora, S., Chamberlain, C., Christophersen, A., Coffey, G. L., Ellis, S. M., Iturrieta, P., Johnson, K. M., Litchfield, N. J., Nicol, A., Milner, K. R., Rastin, S. J., Rhoades, D., Seebeck, H., Shaw, B. E., Stirling, M. W., Wallace, L., Allen, T. I., Bradley, B. A., Charlton, D., Clark, K. J., Fraser, J., Griffin, J., Hamling, I. J., Howell, A., Hudson-Doyle, E., Hulsey, A., Jurgens, V. O., Kaiser, A. E., Kirkman, R., Langridge, R. M., Maurer, J., Rattenbury, M. S., Ristau, J., Schorlemmer, D., Townend, J., Villamor, P., and Williams, C. The Seismicity Rate Model for the 2022 Aotearoa New Zealand National Seismic Hazard Model. *Bulletin of the Seismological Society of America*, 114(1):182–216, Jan. 2024. doi: 10.1785/0120230165.

Gupta, A. and Scholz, C. H. A model of normal fault interaction based on observations and theory. *Journal of Structural Geology*, 22(7):865–879, July 2000. doi: 10.1016/s0191-8141(00)00011-0.

Gómez-Novell, O., García-Mayordomo, J., Ortuño, M., Masana, E., and Chartier, T. Fault System-Based Probabilistic Seismic Hazard Assessment of a Moderate Seismicity Region: The Eastern Betics Shear Zone (SE Spain). *Frontiers in Earth Science*, 8, Dec. 2020. doi: 10.3389/feart.2020.579398.

Heimisson, E. R. Crack to pulse transition and magnitude statistics during earthquake cycles on a self-similar rough fault. *Earth and Planetary Science Letters*, 537:116202, May 2020. doi: 10.1016/j.epsl.2020.116202.

Hergert, T. and Heidbach, O. Slip-rate variability and distributed deformation in the Marmara Sea fault system. *Nature Geoscience*, 3(2):132–135, Jan. 2010. doi: 10.1038/ngeo739.

Herrero-Barbero, P., Álvarez Gómez, J. A., Tsige, M., and Martínez-Díaz, J. J. Deterministic seismic hazard analysis from physics-based earthquake simulations in the Eastern Betics (SE Iberia). *Engineering Geology*, 327:107364, Dec. 2023. doi: 10.1016/j.enggeo.2023.107364.

Iezzi, F., Mildon, Z., Walker, J. F., Roberts, G., Goodall, H., Wilkinson, M., and Robertson, J. Coseismic Throw Variation Across Along-Strike Bends on Active Normal Faults: Implications for Displacement Versus Length Scaling of Earthquake Ruptures. *Journal of Geophysical Research: Solid Earth*, 123(11):9817–9841, Nov. 2018. doi: 10.1029/2018jb016732.

Kim, Y.-S. and Sanderson, D. J. The relationship between displacement and length of faults: a review. *Earth-Science Reviews*, 68 (3–4):317–334, Jan. 2005. doi: 10.1016/j.earscirev.2004.06.003.

Luo, Y., Ampuero, J. P., Galvez, P., Van Den Ende, M., and Idini, B. QDYN: a Quasi-DYNamic earthquake simulator (v1.1), 2017. doi: 10.5281/ZENODO.322459.

Manighetti, I., King, G. C. P., Gaudemer, Y., Scholz, C. H., and Doubre, C. Slip accumulation and lateral propagation of active normal faults in Afar. *Journal of Geophysical Research: Solid Earth*, 106(B7):13667–13696, July 2001. doi: 10.1029/2000jb900471.

Manighetti, I., Campillo, M., Sammis, C., Mai, P. M., and King, G. Evidence for self-similar, triangular slip distributions on earthquakes: Implications for earthquake and fault mechanics. *Journal of Geophysical Research: Solid Earth*, 110(B5), May 2005. doi: 10.1029/2004jb003174.

Manzocchi, T., Walsh, J., and Nicol, A. Displacement accumulation from earthquakes on isolated normal faults. *Journal of Structural Geology*, 28(9):1685–1693, Sept. 2006. doi: 10.1016/j.jsg.2006.06.006.

Marone, C. LABORATORY-DERIVED FRICTION LAWS AND THEIR APPLICATION TO SEISMIC FAULTING. *Annual Review of Earth and Planetary Sciences*, 26(1):643–696, May 1998. doi: 10.1146/annurev.earth.26.1.643.

Mildon, Z. K., Roberts, G. P., Faure Walker, J. P., Beck, J., Papanikolaou, I., Michetti, A. M., Toda, S., Iezzi, F., Campbell, L., McCaffrey, K. J. W., Shanks, R., Sgambato, C., Robertson, J., Meschis, M., and Vittori, E. Surface faulting earthquake clustering controlled by fault and shear-zone interactions. *Nature Communications*, 13(1), Nov. 2022. doi: 10.1038/s41467-022-34821-5.

Mildon, Z. K., Diercks, M., Roberts, G. P., Faure Walker, J. P., Ganas, A., Papanikolaou, I., Sakas, V., Robertson, J., Sgambato, C., and Mitchell, S. Transient Aseismic Vertical Deformation Across the Steeply-Dipping Pisia-Skinos Normal Fault (Gulf of Corinth, Greece). *Tectonics*, 43(8), Aug. 2024. doi: 10.1029/2024tc008276.

Milner, K. R., Shaw, B. E., Goulet, C. A., Richards-Dinger, K. B., Callaghan, S., Jordan, T. H., Dieterich, J. H., and Field, E. H. Toward Physics-Based Nonergodic PSHA: A Prototype Fully Deterministic Seismic Hazard Model for Southern California. *Bulletin of the Seismological Society of America*, 111(2):898–915, Jan. 2021. doi: 10.1785/0120200216.

Nicol, A., Watterson, J., Walsh, J., and Childs, C. The shapes, major axis orientations and displacement patterns of fault surfaces. *Journal of Structural Geology*, 18(2–3):235–248, Feb. 1996. doi: 10.1016/s0191-8141(96)80047-2.

Niroula, G. P., Stirling, M. W., Williams, J., and Gerstenberger, M. Testing and Evaluation of the First-Generation Earthquake Rupture Simulations for New Zealand. *Bulletin of the Seismological Society of America*, 115(5):2263–2278, June 2025. doi: 10.1785/0120250006.

Nixon, C. W., Sanderson, D. J., Dee, S. J., Bull, J. M., Humphreys, R. J., and Swanson, M. H. Fault interactions and reactivation within a normal-fault network at Milne Point, Alaska. *AAPG Bulletin*, 98(10):2081–2107, Oct. 2014. doi: 10.1306/04301413177.

Pace, B., Visini, F., and Peruzza, L. FiSH: MATLAB Tools to Turn Fault Data into Seismic-Hazard Models. *Seismological Research Letters*, 87(2A):374–386, Jan. 2016. doi: 10.1785/0220150189.

Peacock, D. and Sanderson, D. Displacements, segment linkage and relay ramps in normal fault zones. *Journal of Structural Geology*, 13(6):721–733, Jan. 1991. doi: 10.1016/0191-8141(91)90033-f.

Perez-Silva, A., Kaneko, Y., Savage, M., Wallace, L., Li, D., and Williams, C. Segmentation of Shallow Slow Slip Events at the Hikurangi Subduction Zone Explained by Along-Strike Changes in Fault Geometry and Plate Convergence Rates. *Journal of Geophysical Research: Solid Earth*, 127(1), Jan. 2022. doi: 10.1029/2021jb022913.

Perrin, C., Manighetti, I., Ampuero, J., Cappa, F., and Gaudemer, Y. Location of largest earthquake slip and fast rupture controlled by along-strike change in fault structural maturity due to fault growth. *Journal of Geophysical Research: Solid Earth*, 121(5): 3666–3685, May 2016. doi: 10.1002/2015jb012671.

Phillips, T. B., Jackson, C. A.-L., Bell, R. E., Duffy, O. B., and Fossen, H. Reactivation of intrabasement structures during rifting: A case study from offshore southern Norway. *Journal of Structural Geology*, 91:54–73, Oct. 2016. doi: 10.1016/j.jsg.2016.08.008.

Q.G.I.S.Development Team. QGIS Geographic Information System. *Open Source Geospatial Foundation*, 2009. http://qgis.osgeo.org.

Rafiei, M., Khodaverdian, A., and Rahimian, M. A Probabilistic Physics-Based Seismic Hazard Model for the Alborz Region, Iran. *Bulletin of the Seismological Society of America*, 112(4): 2141–2155, May 2022. doi: 10.1785/0120210238.

Ragon, T., Sladen, A., and Simons, M. Accounting for uncertain fault geometry in earthquake source inversions – II: application to the Mw 6.2 Amatrice earthquake, central Italy. *Geophysical Journal International*, 218(1):689–707, Apr. 2019. doi: 10.1093/gji/ggz180.

Roberts, G. P. Fault orientation variations along the strike of active normal fault systems in Italy and Greece: Implications for predicting the orientations of subseismic-resolution faults in hydrocarbon reservoirs. *AAPG Bulletin*, 91(1):1–20, Jan. 2007. doi: 10.1306/08300605146.

Rodriguez Piceda, C. 3D seismic cycle model with variable slip-rate and hazard calculations, 2025. doi: 10.5281/ZENODO.16409390.

Ruina, A. Slip instability and state variable friction laws. *Journal of Geophysical Research: Solid Earth*, 88(B12):10359–10370, Dec. 1983. doi: 10.1029/jb088ib12p10359.

Savage, J. C. A dislocation model of strain accumulation and release at a subduction zone. *Journal of Geophysical Research: Solid Earth*, 88(B6):4984–4996, June 1983. doi: 10.1029/jb088ib06p04984.

Scognamiglio, L., Tinti, E., Casarotti, E., Pucci, S., Villani, F., Cocco, M., Magnoni, F., Michelini, A., and Dreger, D. Complex Fault Geometry and Rupture Dynamics of the MW 6.5, 30 October 2016, Central Italy Earthquake. *Journal of Geophysical Research: Solid Earth*, 123(4):2943–2964, Apr. 2018. doi: 10.1002/2018jb015603.

Shaw, B. E. Beyond Backslip: Improvement of Earthquake Simulators from New Hybrid Loading Conditions. *Bulletin of the Seismological Society of America*, 109(6):2159–2167, Oct. 2019. doi: 10.1785/0120180128.

Shaw, B. E., Milner, K. R., Field, E. H., Richards-Dinger, K., Gilchrist, J. J., Dieterich, J. H., and Jordan, T. H. A physics-based earthquake simulator replicates seismic hazard statistics across California. *Science Advances*, 4(8), Aug. 2018. doi: 10.1126/sciadv.aau0688.

Sieh, K. E. Prehistoric large earthquakes produced by slip on the San Andreas Fault at Pallett Creek, California. *Journal of Geophysical Research: Solid Earth*, 83(B8):3907–3939, Aug. 1978. doi: 10.1029/jb083ib08p03907.

Tapponnier, P., Ryerson, F. J., Van der Woerd, J., Mériaux, A.-S., and Lasserre, C. Long-term slip rates and characteristic slip: keys to active fault behaviour and earthquake hazard. *Comptes Rendus de l'Académie des Sciences - Series IIA - Earth and Planetary Science*, 333(9):483–494, Nov. 2001. doi: 10.1016/s1251-8050(01)01668-8.

Tarquini, S., Isola, I., Favalli, M., Mazzarini, F., Bisson, M., Pareschi, M. T., and Boschi, E. TINITALY/01: a new Triangular Irregular Network of Italy. *Annals of Geophysics*, 50(3):407–425, Dec. 2007. doi: 10.4401/ag-4424.

Tarquini, S., Isola, I., Favalli, M., Battistini, A., and Dotta, G. TINITALY, a digital elevation model of Italy with a 10 meters cell size, version 1.1, 2023. doi: 10.13127/TINITALY/1.1.

Tavakolizadeh, N., Mohammadigheymasi, H., Visini, F., and Pombo, N. FaultQuake: An open-source Python tool for estimating Seismic Activity Rates in faults. *Computers & Geosciences*, 191:105659, Sept. 2024. doi: 10.1016/j.cageo.2024.105659.

Valentini, A., Visini, F., and Pace, B. Integrating faults and past earthquakes into a probabilistic seismic hazard model for peninsular Italy. *Natural Hazards and Earth System Sciences*, 17 (11):2017–2039, Nov. 2017. doi: 10.5194/nhess-17-2017-2017.

Wang, B. and Barbot, S. Rupture segmentation on the East Anatolian fault (Turkey) controlled by along-strike variations in long-term slip rates in a structurally complex fault system. *Geology*, 52(10):779–783, July 2024. doi: 10.1130/g52403.1.

Wedmore, L. N. J., Faure Walker, J. P., Roberts, G. P., Sammonds,

P. R., McCaffrey, K. J. W., and Cowie, P. A. A 667 year record of coseismic and interseismic Coulomb stress changes in central Italy reveals the role of fault interaction in controlling irregular earthquake recurrence intervals. *Journal of Geophysical Research: Solid Earth*, 122(7):5691–5711, July 2017. doi: 10.1002/2017jb014054.

Wells, D. L. and Coppersmith, K. J. New empirical relationships among magnitude, rupture length, rupture width, rupture area, and surface displacement. *Bulletin of the Seismological Society of America*, 84(4):974–1002, Aug. 1994. doi: 10.1785/bssa0840040974.

Williams, J. N., Werner, M. J., Goda, K., Wedmore, L. N. J., De Risi, R., Biggs, J., Mdala, H., Dulanya, Z., Fagereng, A., Mphepo, F., and Chindandali, P. Fault-based probabilistic seismic hazard analysis in regions with low strain rates and a thick seismogenic layer: a case study from Malawi. *Geophysical Journal International*, 233(3):2172–2207, Feb. 2023. doi: 10.1093/gji/ggad060.